Atmos. Chem. Phys., 7, 4027–4042, 2007
www.atmos-chem-phys.net/7/4027/2007/
© Author(s) 2007. This work is licensed
under a Creative Commons License.

Atmospheric Chemistry and Physics

Atmospheric effects of volcanic eruptions as seen by famous artists and depicted in their paintings

C. S. Zerefos[1,2], V. T. Gerogiannis[3], D. Balis[4], S. C. Zerefos[5], and A. Kazantzidis[4]

[1]National Observatory of Athens, Athen, Greece
[2]Academy of Athens, Athen, Greece
[3]National Meteorological Service, Athen, Greece
[4]Laboratory of Atmospheric Physics, Aristotle University of Thessaloniki, Thessaloniki, Greece
[5]School of Architecture, National Technical University of Athens, Athen, Greece

Received: 26 February 2007 – Published in Atmos. Chem. Phys. Discuss.: 16 April 2007
Revised: 12 July 2007 – Accepted: 26 July 2007 – Published: 2 August 2007

Abstract. Paintings created by famous artists, representing sunsets throughout the period 1500–1900, provide proxy information on the aerosol optical depth following major volcanic eruptions. This is supported by a statistically significant correlation coefficient (0.8) between the measured red-to-green ratios of a few hundred paintings and the dust veil index. A radiative transfer model was used to compile an independent time series of aerosol optical depth at 550 nm corresponding to Northern Hemisphere middle latitudes during the period 1500–1900. The estimated aerosol optical depths range from 0.05 for background aerosol conditions, to about 0.6 following the Tambora and Krakatau eruptions and cover a period practically outside of the instrumentation era.

1 Introduction

Man-made forcing of climate change is complicated by the fact that it is superimposed on natural climate variability. This natural variability on decadal to century time scales includes, among others, the variability in volcanic stratospheric aerosols and atmospheric transparency. Intense optical phenomena observed worldwide during sunsets following major volcanic eruptions, caused by volcanic aerosols injected in the stratosphere which remained there for a period of few years after the eruption, have been reported by several authors (Symons, 1888; Sandick, 1890; Sapper, 1917; Shaw, 1936; Hymphreys, 1940; Lamb, 1970; Deirmendijian, 1973). Prominent among them are the eruptions of Awu (Indonesia-1641), Katla (Iceland-1660), Tongkoko (Indonesia-1680), Laki (Iceland-1783), Tambora (Indonesia-1815), Babuyan (Philippines-1831), Coseguina (Nicaragua-1835), and Krakatau (Indonesia-1680, 1883). These optical phenomena have been attributed to the enhanced forward scattering caused by the volcanic aerosols in the stratosphere (Deirmendijian, 1973).

The effects of volcanic eruptions on climate along with volcanic indices of importance to climate have been recently discussed in the literature (Robock, 2000; Zielinski, 2000; Robertson et al., 2001). Volcanic aerosol indices include the Dust Veil Index (DVI), the Volcanic Explosivity Index (VEI) as well as ice core sulphate Index which can go back to 1500 (Lamb, 1970; Zielinski, 2000; Newhall and Self, 1982).

The earliest compilation is the DVI, introduced by Lamb (1970, 1977, 1983). It extends from 1500 to 1983 and is based primarily on historical accounts of optical phenomena while surface radiation measurements were used when available. In a few cases, reports of cooling associated with volcanic aerosols were incorporated into the index. Robock (1981) introduced a latitudinally dependent estimation of the DVI. Sato et al. (1993) produced a zonally averaged compilation of optical depth for volcanic eruptions from 1850. The observational sources of this data set are similar to the DVI in addition to land-based pyrheliometric measurements of atmospheric extinction for the period after 1882. Stothers (1996) has improved upon the Sato et al. (1993) reconstruction for the period 1881–1960 by incorporating more pyrheliometric data from stations primarily in the Northern Hemisphere. Stothers (1996) also used historical accounts of starlight extinction, purple twilight glows, and other turbidity indicators to support and expand upon the pyrheliometric data.

Ice cores offer another valuable opportunity to reconstruct volcanic aerosols through the measurements of volcanic sulfate (SO_4^{2-}) deposited on glacial ice in the years immediately following an eruption. Portions of the technique were initially developed by Hammer et al. (1980) and Clausen and Hammer (1988). They used the record of bomb fallout in Greenland to obtain a mass of H_2SO_4 produced in the stratosphere from an individual eruption. They then accounted for the latitude of the eruption by employing an appropriate

Correspondence to: C. S. Zerefos
(zerefos@geol.uoa.gr)

Published by Copernicus Publications on behalf of the European Geosciences Union.

multiplier within the calculations. Zielinski (1995) expanded on the technique by calculating the total H_2SO_4 aerosol loading and then ultimately, the optical depth (τ_D) using the relationship defined by Stothers (1984a). However, when the resulting ice core-derived τ-values for the GISP2 (Greenland Ice Sheet Project Two) core were calibrated with other independent optical depth measurements it was found that equivalent optical depth measurements were obtained in some cases, but the ice core estimates were 2–5 times greater in others. This was especially true for mid-latitude northern hemisphere eruptions where there may have been some tropospheric transport of H_2SO_4 to polar ice sheets, and thus an enhanced signal. The high temporal resolution (annual to biennial), the length of the records, and the low temporal error (e.g. ± 2 years for uppermost part of the GISP2 core) available in many ice core records allow for the reliable quantification of the atmospheric impact of past volcanism prior to the period of reliable historical observations. The GISP2 ice core has been used to create a 2100-year record of stratospheric loading and optical depth estimates. Robock and Free (1995, 1996) pioneered the use of sulfate data from multiple ice cores to construct a record of volcanic activity. Robertson et al. (2001) produced a high-resolution time and latitude-dependent estimate of stratospheric optical depth stretching back to 1500 by combining historical observations, ice core data from both Greenland and Antarctica, as well as recent satellite data. They also incorporated ice core data that were unavailable for the previous reconstructions and avoided ice cores that were less well dated or strongly complicated by non-volcanic aerosols.

The present work aims at providing a new look at the reconstruction of the aerosol optical depth before, during and after major volcanic eruptions by studying the coloration of the atmosphere in paintings which portrayed sunsets in the period 1500–1900, i.e. when atmospheric observations were scarce and mostly non-existent. This was done by measuring the red to green ratios of more than 500 paintings as well as using model calculations to simulate and calibrate the measurements from the coloration in paintings as described in the following text.

2 Methodology

2.1 Criteria in selecting paintings

Paintings representing sunsets throughout the period 1500–1900 form the source of the observational material in this study. Most of these paintings were available in digital form at the official web sites of 109 museums and galleries (see http://www.noa.gr/artaod for more details). In the 400-year period of study (1500–1900) eleven major volcanic eruptions have been observed characterized by DVI larger than 250 (Lamb, 1970). In that same period, but only for eight of these eruptions, we have found a number of 554 paintings from 181 painters, which have been divided into two groups: the group of "volcanic sunset paintings" and the group of "non-volcanic sunset paintings". The "volcanic sunset paintings" include those that were created within a period of three years that followed a major volcanic eruption. The rest of the paintings were considered to represent the background coloration of sunsets. Fifty four "volcanic sunset paintings" were found from 19 painters that fulfilled the above criteria and each of them was dated. Notable among the painters are Claude Lorrain, John Singleton Copley, Friedrich Caspar David, Joseph Mallord William Turner, Breton Jules, Edgar Degas, Alexander Cozens and Gustav Klimt. A complete list of all painters and paintings considered in this study can be found at http://www.noa.gr/artaod. A number of these paintings have not been included because of lack of information on the date of their creation.

2.2 Chromatic ratio

In order to characterize the redness of the sunset sky, the chromatic ratio R/G was calculated from the RGB values measured on the digitized paintings and when possible, also the solar zenith angle pertaining to each painting. For the calculation of the R/G ratio we averaged the measured values over the field of view of the artist near the horizon. Red, so as green, yellow and blue, is a unique hue and by definition it cannot be described by the other unique hue alone or in combination (Wyszecki and Stiles, 1982). Each unique hue refers to the perceptual experience of that hue alone. Perceptual opponency of red/green forms the conceptual basis for quantifying the redness of monochromatic light. In a classic study, Jameson and Hurvich (Jameson and Hurvich, 1955) reasoned that the amount of redness in a monochromatic light can be measured by combining it with a second light that appears green when viewed alone (Shevell, 2003). It should be noted that color appearance is reasonably stable with increasing age of the painter (Schefrin and Werner, 1990). Therefore, it is expected that abnormalities seen in time series of R/G values for each painter cannot be attributed to digression of the painters colour acuity due to age and could present colour perception of real natural abnormalities, such as those following eruptions, or abnormalities caused by psychological or cultural reasons. Thus R/G ratios can provide information on the perception of colours by the painter which are practically independent of aging and therefore they may be suitable to examine deviations of R/G values from those that correspond to background atmospheric conditions at the time of the creation of the work of art.

2.3 Model description

In this study, the UVspec model (Mayer and Kylling, 2005; Kylling et al., 1998) from the LibRadTran package (http://www.libradtran.org) was used to simulate the R/G ratios determined from the paintings. The model uses the

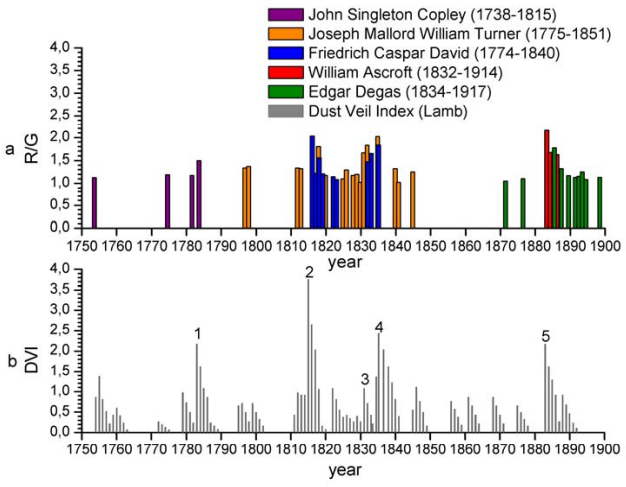

Fig. 1. (a) The variation of the chromatic ratio R/G that correspond to paintings of Copley, Turner, David, Ascroft and Degas. **(b)** The Dust Veil Index. The numbered peaks are 1. Laki, 2. Tambora, 3. Babuyan, 4. Coseguina and 5. Krakatau.

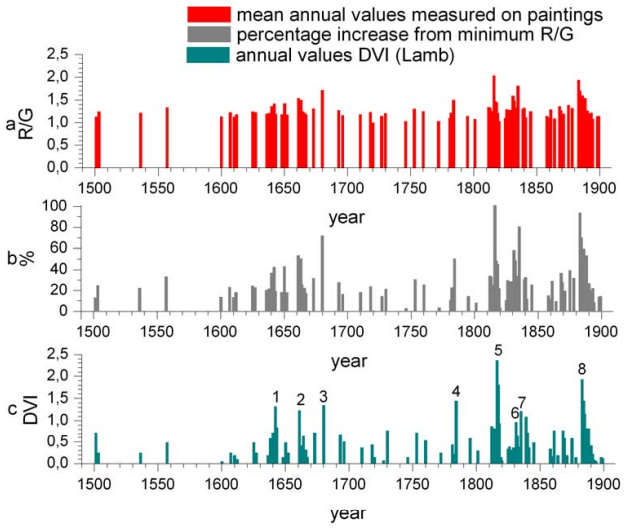

Fig. 2. (a) The mean annual value of R/G measured on 327 paintings. **(b)** The percentage increase from minimum R/G value shown in (a). **(c)** The corresponding Dust Veil Index (DVI). The numbered picks correspond to different eruptions as follows: 1. 1642 (Awu, Indonesia-1641), 2. 1661 (Katla, Iceland-1660), 3. 1680 (Tongkoko & Krakatau, Indonesia-1680), 4. 1784 (Laki, Iceland-1783), 5. 1816 (Tambora, Indonesia-1815), 6. 1831 (Babuyan, Philippines-1831), 7. 1835 (Coseguina, Nicaragua-1835),. 8. 1883 (Krakatau, Indonesia-1883).

pseudo-spherical DISORT (Stamnes et al., 1988) to solve the radiative transfer equation using 16 streams. Irradiance and radiance spectra were calculated at 10 nm resolution and for the 15- to 85 degrees of solar zenith angle. The atmospheric composition and structure as used in the model was based on vertical profiles taken from the literature. The AFGL midlatitude winter profiles were used for ozone, temperature and air pressure (Anderson et al., 1986). Rayleigh scattering cross-sections were calculated according to the analytic function proposed by Nicolet (1984). In this paper we calculated the direct and diffuse irradiance for the visible wavelength range (400–700 nm) for four stratospheric aerosol scenarios, keeping all other input parameters constant. The aerosol scenarios considered were a background stratospheric profile of the aerosol extinction and three aerosol profile that corresponds to moderate, high and extreme volcanic dust. The runs were repeated for AOD values at 550 nm from 0 to 2 with a step of 0.01. From the above model runs estimates of the R/G ratios were determined by the model for various combinations of the aerosol model and the aerosol optical depth, and these estimates were compared to the ones that obtained from the paintings. The R/G ratio was approximated using the ratio of the diffuse irradiance of two wavelengths (550 nm and 700 nm) rather than the radiance. The reason for using this approximation is discussed in more detail in Sect. 3.4. This comparison allowed us to associate to each painting an estimate of the aerosol optical depth during the time of creation.

3 Results and discussion

3.1 Chromatic ratios in art paintings at sunset versus DVI

Our analysis began by examining the artist's perception of sunsets by measuring chromatic ratios during each artist's lifetime. Very few artists have painted sunsets before, during and following major volcanic eruptions. We found only 5 painters which in their lifetime have painted sunsets in all these three categories. The time series of the R/G ratios for these five discreet painters is shown in Fig. 1 together with the corresponding series of DVI. We can see from Fig. 1 for example, that John Singleton Copley has "painted" an enhancement of 33% relative to a minimum R/G value in 1784. Joseph Mallord William Turner "painted" enhancements of 76.7% in 1818, 79.2% in 1832 and 97,7% in 1835, while Friedrich Caspar David observed enhancements of 89.5% in 1816, 51.3% in 1833 and 41.2% in 1835. Similarly Edgar Degas observed an enhancement of 68.4% in 1885. As can be seen from Fig. 1 the R/G value measured on paintings corresponding to a volcanic event, are 1.3–1.4 times greater than the R/G values before and after the event. Therefore, the observed departures of R/G chromatic ratios seen in Fig. 1, which coincide in time with major volcanic eruptions, can be tentatively attributed to the volcanic events and not to abnormalities in the color degradation due to age or other random factor affecting each painter's color perception. Figure 2

Table 1. Estimated aerosol optical depth at 550 nm corresponding to middle latitudes for each major volcanic eruption from this papers in comparison with other studies.

	Volcano Name	Year of the eruption	AOD this study	Nearest estimate from other studies
1	Awu	1641	0.35	0.33 (Zielinski, 2000)
2	Katla	1660	0.29–0.34	N/A
3	Tongkoko & Krakatau	1680	0.47	N/A
4	Laki	1783	0.30	0.21–0.28 (Robertson et al.,2001) 0.19 (Robock and Free, 1996) 0.12 (Zielinski, 2000)
5	Tambora	1815	0.33–0.60	0.5 (Robertson et al., 2001) 0.5 (Robock and Free, 1996) 0.2–0.9 (Stothers, 1996)
6	Babuyan	1831	0.28–0.29	0.24 (Zielinski, 2000)
7	Coseguina	1835	0.52	0.11–0.21 (Robertson et al., 2000)
8	Krakatau	1883	0.37-0.57	0.6 (Deirmendijian, 1973)

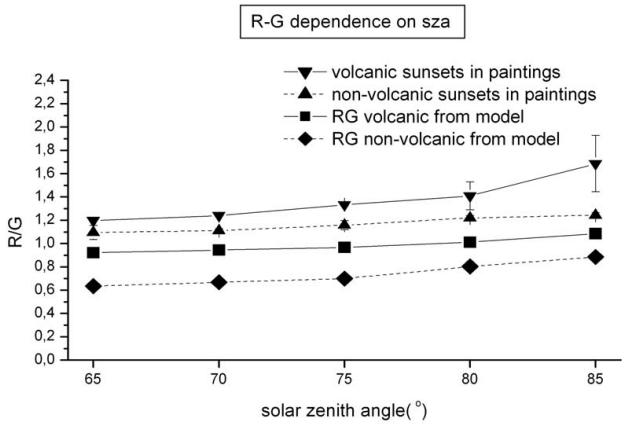

Fig. 3. The dependence of the chromatic ratio R/G on solar zenith angle as estimated from the paintings and the model. The volcanic sunset values include sunsets that were painted within a period of 3 years following a volcanic eruption. The non-volcanic sunsets include the remaining paintings at least 3 years apart from a volcanic eruption. The modeled R/G diffuse irradiance (R=700 nm, G=550 nm) calculated for background aerosol and high volcanic aerosol.

shows mean annual values of R/G sunset ratios measured from paintings along with the percentage increase from the absolute minimum R/G value in the series (middle curve) together with the corresponding DVI values during 1500–1900. We note here that Fig. 2 includes 327 paintings, from a total of 554 examined, that fulfilled the criteria mentioned before and that their date could be determined or estimated. From that figure we see an enhancement of mean annual R/G relative to the absolute minimum R/G value. The numbered picks in that figure correspond to different eruptions as follows: 1. 1642 (Awu, Indonesia-1641), 2. 1661 (Katla, Iceland-1660), 3. 1680 (Tongkoko & Krakatau, Indonesia-1680), 4. 1784 (Laki, Iceland-1783), 5. 1816 (Tambora, Indonesia-1815), 6. 1831 (Babuyan, Philippines-1831), 7. 1835 (Coseguina, Nicaragua-1835),. 8. 1883 (Krakatau, Indonesia-1883). As seen from Fig. 2, there is a remarkable correspondence between peaks in R/G values in years close to those with major volcanic eruptions. The linear correlation coefficient between mean annual R/G values and DVI was found to be r=0.827 based on 88 pairs, which is of high statistical significance.

3.2 Dependence of the chromatic ratio on the solar zenith angle

The dependence of R/G ratios on solar zenith angle was studied by measuring the zenith angle with the following method: Wherever the exact date (time, day, year) and place of the painting is known, the solar zenith angle was computed. When that information was not available, the elevation of the sun was measured from the horizon and with the help of a fixed reference point on the painting, the solar zenith angle was calculated trigonometrically. In cases of uncertainty and when possible, the geometry of shadows provided additional help in approximating the solar zenith angle.

Figure 3 presents the variation of the measured R/G ratios versus the solar zenith angle averaged in 5° bins, for the two groups of volcanic and non-volcanic sunset paintings. In addition Fig. 3 shows the R/G ratios calculated from the model for the same solar zenith angles. The model calculates the diffuse irradiance ratio R/G computed for background aerosols and high volcanic aerosols. The wavelengths used are: R=700 nm and G=550 nm. Both in paintings and the model, the R/G ratio in the volcanic sunsets is higher than

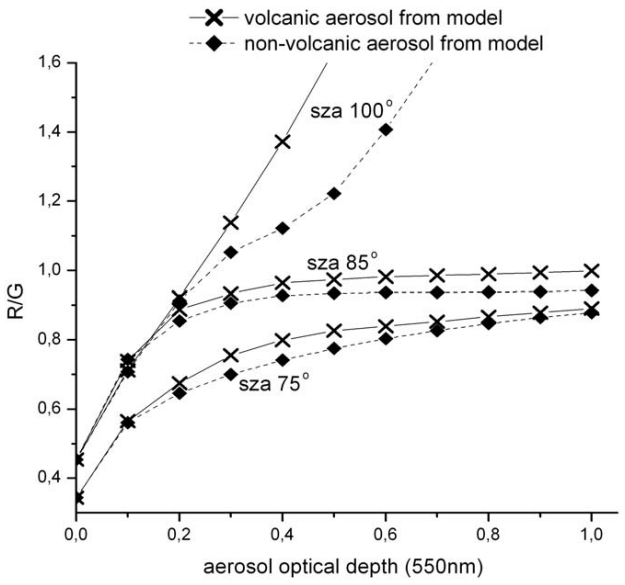

Fig. 4. Nomogramm of R/G and aerosol optical depth as resulted from the model for three solar zenith angles calculated for non-volcanic and volcanic aerosols used to calibrate the measurements on paintings.

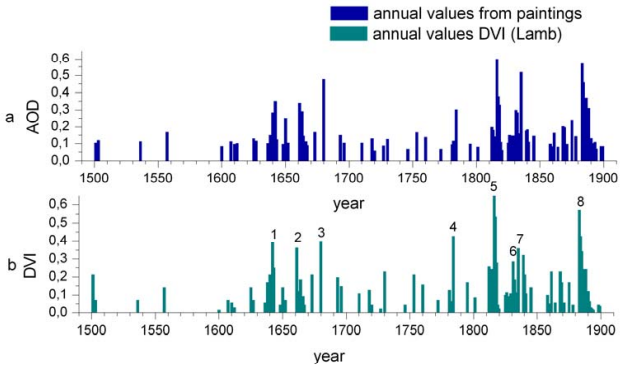

Fig. 5. (a) The aerosol optical depth at 550 nm as estimated from paintings and model calculations. **(b)** The corresponding Dust Veil Index. The numbers on the DVI histogram refer to the same major volcanic eruptions outlined in Fig. 2.

the non-volcanic. This can be explained by Mie scattering, caused by the sulfate aerosol particles that are about the same size as the wavelength of visible light, which enhances the scattered radiation in the forward direction (Robock, 2000). For solar zenith angles greater than 80° the chromatic ratio R/G in the paintings is 1.4 times greater than the non-volcanic. The model shows that the ratio R/G due to extreme volcanic aerosols is 1.45 to 1.25 larger when compared to the ratio calculated for the background aerosols. As we see from Fig. 3, the model results when compared to the measured R/G ratios on paintings show a systematic bias of about 30%. The possible source for this bias is discussed in detail in section 3.4. This bias was also confirmed by examining R/G ratios for "Krakatau" paintings, and from other measurements and our estimates of the optical depth of the volcanic debris. This was done by measuring R/G ratios in W. Ascroft color drawings of sunsets which followed Krakatau in London (Symons, 1888). These color drawings have been constructed at known solar zenith angles of 92.6° and 99.5°, as calculated from time, date and month and London's geographical coordinates.

3.3 Estimates of optical depth

To estimate the optical depth which could be attributed to each volcanic eruption, a nomogram of R/G values and aerosol optical depth was constructed for volcanic and non-volcanic aerosols using the UVspec model for three solar zenith angles as seen in Fig. 4. Before that the observed arbitrary R/G ratios have been adjusted for the systematic bias discussed in the previous paragraph. The estimate of the aerosol optical depth was done by converting the R/G measurements on paintings at a given solar zenith angle through the nomogram of Fig. 4 to optical depth at 550 nm. At the paintings where the sun was under the horizon and the calculation of the solar zenith angle was not possible, we hypothesized it to be 100°.

Figure 5a shows the time series of the aerosol optical depth from all paintings using the method described above along with the time series of DVI for the 400-year period 1500–1900. The estimated aerosol optical depth ranged from 0.05 for background aerosol conditions at middle latitudes of the northern hemisphere, up to 0.6 which corresponds to the Tambora eruption. The numbers on the DVI histogram refer to the same major volcanic eruptions outlined in Fig. 2. Table 1 summarizes the aerosol optical depth as estimated in this study from paintings which is found to be in reasonable agreement with independent estimates by other authors. Robock and Free (1996) estimated that the aerosol optical depth for Laki has a value of 0.19 while Robertson et al. (2001) give 0.16. Both papers (Robertson et al., 2001; Robock and Free, 1996) give to Tambora the value of 0.50, while Stothers (1984b) calculated the global optical depth to be 0.85 in 1815, 0.9 in 1816 and 0.2 in 1817. For 1831 and 1835 Robock and Free (1996) estimated an optical depth of 0.09 and 0.11 and Robertson et al. (2001) of 0.07 and 0.18 respectively. For the Krakatau eruption, Sato et al. (1993) estimated the optical depth to be about 0.13, Stothers (1996) gives 0.14 in 1884 decreasing to 0.02 by 1886, Robock and Free (1996) give 0.12 and Robertson et al. (2001) 0.09, while Dermidijian (1973) estimates an AOD of about 0.6. As seen in Fig. 6 the correlation coefficient between AOD and DVI is 0.87 again remarkably significant and points out to the important information that can be extracted from paintings portaging natural phenomena, which attracted the attention of famous painters, although probably most of them did not know anything about their occurrence.

Table 2. Error in AOD estimates derived from the average R/G variability within a painting (±0.014 according to table A1).

Solar Zenith angle	AOD	Error
75	0.1	< 0.05
	0.5	0.06 to 0.12
85	0.1	< 0.05
	0.5	0.1 to 0.18

3.4 Error sources and uncertainties of the AOD estimates

There are many sources of uncertainties both in the experimental determination of the R/G ratios as well as in the model calculations, which both affect the accuracy of the AOD estimates. Concerning the extraction of the R/G ratios from digital images of paintings the following sources of uncertainty can be identified: The use of different cameras, the use of flash or natural light, different exposure times between different shots may produce different digital versions for the same painting. In order to make an estimate how these different techniques might affect the measured R/G ratios in a digital image, we conducted a simple experiment where we photographed the same sunset image with two different digital cameras, using natural light and different exposure times. Then these images were analysed in a similar manner as the paintings.

The resulted differences in the R/G ratios were very small (less than 0.01) and smaller than the variability of the R/G within the digital image. We note here however, that the remarkable high correlation found between the R/G ratios and the DVI strongly indicate that such possible small uncertainties might cancel out when we consider ratios obtained with different cameras, since use of flashes is not applicable in digital photos of paintings. Other source of uncertainty in the R/G values is their variability within a painting/image, which also largely depends on the area selected to measure on the painting. According to table A1 (see Appendix A) this variability is the order of 0.014 (mean error value). This range of uncertainty in the determination of R/G affects also our ability to retrieve from these ratios estimates of AOD. Tables 2 and 3 show the expected uncertainty in the estimated AOD due to the variability of the R/G ratios within a painting and to uncertainties in determining the SZA. These errors are given for different AOD and SZA values. The uncertainty is less than 0.05 for small optical depths and smaller SZA. This number is comparable to the accuracy of other experiment measurements of AOD. The error however increases with increasing AOD and SZA and can be as large as 0.18 for AOD larger than 0.5.

Our model estimates of the R/G ratios are approximations and include systematic sources of errors or bias. There are mainly two sources of systematic bias in our calculations.

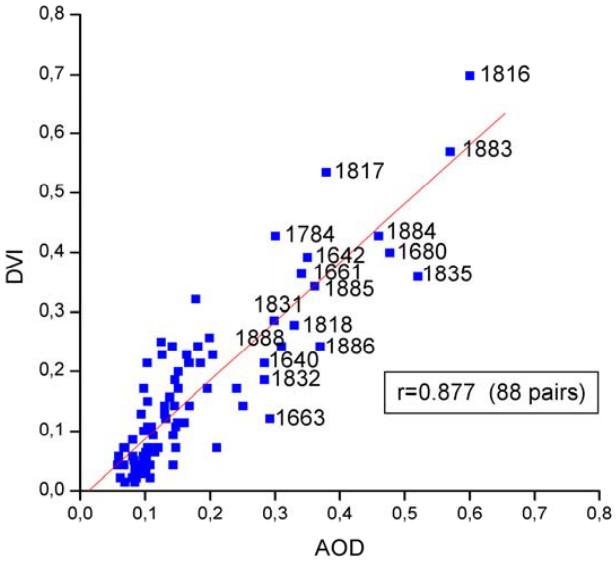

Fig. 6. Linear correlation between annual mean aerosol optical depth at 550 nm, estimated from sunset paintings following volcanic eruptions, and mean annual values of DVI. The errors in the AOD are less than 0.05 for values around 0.1 and can be up to 0.18 for AOD values greater then 0.5.

Table 3. Error in AOD derived from a typical error in estimating the SZA in a painting within ±2°.

Solar Zenith angle	AOD	Error
75	0.1	< 0.05
	0.5	0.07
85	0.1	< 0.05
	0.5	< 0.05

The first concerns the use of RGB values directly calculated from the libRadtran model using the CIE color matching functions (Mayer and Emde, 2007). These R/G ratios are systematically higher (about 0.1) than those calculated from the ratio of two wavelengths for SZAs smaller than 85deg. Another source of systematic bias is the type of radiometric calculations performed. In our calculations we used the diffuse irradiance over the whole hemisphere at the given wavelengths. However if we calculate the R/G ratios shown in Figs. 1 and 2 using the integral of the calculated radiances within 20° azimuth, around the setting sun and for zenith angles 70–90deg, then we would be able to simulate with the model the paintings' ratios even better. We note here that the radiative transfer solver included in libRadtran is only a pseudo-spherical and not a fully spherical code, and therefore its accuracy for radiance calculations is limited at high SZAs. The values based on the radiance calculations are considerably higher (20–30%) than those shown in Fig. 3, both for

volcanic and non volcanic conditions. For high AOD values (>0.5) the results from the model and the paintings are very close and thus most of the bias is eliminated when one uses the radiances for the calculation of the R/G ratios. However we did not extend our sensitivity tests for higher zenith angles since the usefulness of radiance values for the retrieval is determined by the increased uncertainty of the 1-D radiative transfer model for high solar zenith angles.

4 Conclusions

In this work we have attempted to estimate the aerosol optical depth following major volcanic eruptions as well as to provide evidence of the variability of the background atmospheric optical depth at 550 nm in a 400-year period, estimated from the coloration of sunsets in famous art paintings. These reconstructed AOD timeseries provide the advantage, compared to DVI and other indices, that they can be directly used in models for radiative forcing calculations for periods with no measurements available. The reconstructed data can be compared with current (20th century) measurements of AOD, to provide estimates of long-term variability of background AOD during a period of about 500 years. These estimates can be useful to detect changes related to air pollution over Europe's middle latitudes.

The results presented show a strong dependence of the chromatic R/G ratios perception by the painters on the scattering state of the atmosphere. The artists for the 400-year period under study (1500–1900) appear to have simulated the colours of nature with a remarkable precise coloration as proved by the unexpected high correlation coefficient of 0.83 found between the well known index of volcanic activity (DVI) and the values of the coloration depicted in the sunset paintings. A time series of aerosol optical depth at 550 nm has been compiled, representing the middle latitudes of the Northern Hemisphere and covers the periods 1500–1900. The aerosol optical depth estimated ranged from 0.05, for background aerosol conditions, up to about 0.6 which corresponded to the period after the Tambora and Krakatau eruptions. These estimates are in reasonable agreement with independent studies referring to the same period. We should note here that because of the controversy on the date that the famous painting "The Scream" was created by Edvard Munch prevented us to use it as sample. This is because while Robock (2000) attributes it to the 1892 Awu eruption, Olson (2004) shows topographically that it was created about ten years before, in the winter of 1883-84. The high R/G value of "The Scream" (over 2.10), as well as similar high values of other paintings by Edvard Munch (e.g. "Despair" and "Anxiety") are possible indications illustrating the memory kept by the painter of the coloration of the optical phenomena which he saw following the 1883 Krakatau event.

At any rate, we believe that this study will form the basis for more research to be done on environmental information content in art paintings. Through the eyes of painters and other artists it is expected to get information on past natural phenomena that have escaped attention of scholars until now. As J. M. W. Turner (Bockemuhl, 2000) said: *"I did not paint it to be understood, but I wished to show what such a scene was like"*.

Appendix A

Examples of "volcanic" and "non-volcanic" paintings considered in the paper

Fig. A1. Example of a non-volcanic sunset, painted by J.M.W. Turner entitled "The Lake, Petworth, Sunset", created in 1828, with R/G ratio of 1.14±0.04 (see Tate Gallery at http://www.tate.org.uk/servlet/ViewWork?cgroupid=999999996{\&}workid=14876).

Fig. A2. Example of volcanic sunset by J. M. W. Turner entitled "Sunset" (c.1833) with R/G ratio of 1.76±0.03, that illustrate the optical phenomena due to the eruption of Babuyan (1831) (see Tate Gallery at http://www.tate.org.uk/servlet/ViewWork?cgroupid=999999996{\&}workid=14820).

Appendix B

Art paintings and measured R/G values

Table B1. Prospective users of AOD values are kindly requested to contact zerefos@geol.uoa.gr prior to any use.

Painter's Name	Title of Painting	Year	R/G	SZA	AOD	Gallery*
Gerard David	God the Father Blessing	1506	1.16±0.01	999	0.1	LVR
Tiziano Vecellio	Girl with a Basket of Fruits	1557	1.31±0.03	95	0.15	STL
Jan Brueghel the Elder	Landscape with Windmills	1607	1.22±0.05	999	0.12	PRD
Peter Paul Rubens	The Four Philosophers	1612	1.06±0.02	999	0.07	PLP
Hendrick Terbrugghen	St Sebastian Tended by Irene and her Maid	1625	1.24±0.03	100	0.12	AMA
Sir Anthony van Dyck	Portrait of the Painter Cornelis de Wae	1627	1.22±0.01	999	0.12	RBA
Rembrandt	The Risen Christ Appearing to Mary Magdalen	1638	1.03±0.02	85	0.06	RCL
Gellee, Claude (Le Lorrain)	Imaginary View of Tivoli	1642	1.49±0.06	85	0.36	CTI
Gellee, Claude (Le Lorrain)	Italian Coastal Landscape	1642	1.38±0.09	83	0.37	STL
Nicolaes Pietersz Berchem	Landscape with Jacob, Rachel, and Leah	1643	1.13±0.02	86	0.14	LVR
Gellee, Claude (Le Lorrain)	Harbour Scene at Sunset	1643	1.17±0.02	87	0.17	RCL
Gellee, Claude (Le Lorrain)	Landscape with Paris and Oenone	1648	1.13±0.01	82	0.09	LVR
Gellee, Claude (Le Lorrain)	Seaport with the Embarkation of the Queen of Sheba	1648	1.14±0.03	85	0.09	NGL
Gellee, Claude (Le Lorrain)	Ulysses Returns Chryseis to her Father	1648	1.16±0.02	82	0.09	LVR
Jacob Adriaensz Backer	Venus and Adonis	1650	1.41±0.04	999	0.18	SFS
Cuyp Aelbert	Herdsman with Cows by a River	1650	1.05±0.00	71	0.17	NGL
David Teniers the Younger	Flemish Kermess	1652	1.19±0.04	92	0.1	RBA
Gellee, Claude (Le Lorrain)	Landscape with the Rest on the Flight into Egypt	1661	1.21±0.01.	80	0.34	HMT
Jan de Bray	Pharaoh's Daughter with Her Attendants and Moses in the Reed Basket	1661	1.52±0.04	999	0.28	BVB
Gellee, Claude (Le Lorrain)	Landscape with Tobias and the Angel	1663	1.48±0.02	84	0.29	HMT
Ludolf Backhuysen	Ships in Distress off a Rocky Coast	1667	1.17±0.02	69	0.23	NGA
Wright John Michael	Sir Neil O'Neill	1680	1.71±0.04	93	0.47	NGA
Jacob de Heusch	River View with the Ponte Rotto	1696	1.15±0.02	66	999	HAU
Louis Philippe Boitard	An Exact Representation of the Game Cricket	1760	1.21±0.02	999	0.11	TTG
James Lambert	Landscape	1769	1.14±0.01	90	0.09	NGL
John Singleton Copley	Watson and the Shark	1778	1.07±0.04	65	999	FAB
De Loutherbourg, Philip James	Travellers Attacked by Banditti	1781	1.10±0.01	69	999	TTG
Jakob Philipp Hackert	Landscape with a Ancient Festival	1781	1.11±001	76	0.2	HMT
Thomas Gainsborough	Girl with Pigs	1782	1.23±0.02	999	0.13	CHW
John Singleton Copley	Mrs. Daniel Denison Rogers	1784	1.66±0.16	86	0.32	FGA
Jakob Philipp Hackert	View of Caserta	1784	1.09±0.01	55	999	HMT
Sir Joshua Reynolds	Lady Elizabeth Foster	1787	1.70±0.03	100	0.27	TTG
Jakob Philipp Hackert	Italian Landscape	1795	1.14±0.04	76	0.25	HMT
Joseph Mallord William Turner	A Road Crossing a River; Sunset Sky Seen beyond Trees	1798	1.11±0.02	82	0.08	TTG
Jean Broc	The Death of Hyacinth	1801	1.08±0.01	90	0.07	RPC
Joseph Mallord William Turner	Distant View of Whitby from the Moors: A Windmill against a Sunset Sky; The Abbey Beyond	1801	1.07±0.02	86	0.07	TTG
Joseph Anton von Koch	The Monastery of San Francesco di Civitella in the Sabine Mountains	1812	1.29±0.03	90	0.19	HMT

Table B1. Continued.

Painter's Name	Title of Painting	Year	R/G	SZA	AOD	Gallery*
Karl Friedrich Schinkel	The Banks of the Spree near Stralau	1817	1.29±0.01	90	0.19	NGB
Caspar David Friedrich	Griefswald in the Moonlight	1817	1.12±0.05	100	0.14	NGO
Joseph Mallord William Turner	The Decline of the Carthaginian Empire	1817	1.27±0.03	74	0.46	TTG
Caspar David Friedrich	Two Men by the Sea at Moonrise	1817	1.26±0.14	100	0.19	NGB
Theodore Gericault	Landscape with Acqueduct	1818	1.23±0.00	81	0.36	MMA
Caspar David Friedrich	Woman in front of the Setting Sun	1818	1.64±0.09	92	0.32	FLK
Caspar David Friedrich	Wanderer Looking over the Sea of Fog	1818	1.11±0.00	999	0.14	KNH
Joseph Mallord William Turner	The Roman Campagna from Monte Testaccio, Sunset	1819	1.05±0.01	76	0.23	TTG
Joseph Mallord William Turner	Moonlight over the Campagna	1819	1.06±0.01	999	0.07	TTG
Joseph Mallord William Turner	St. Peter's from the South	1819	1.38±0.02	78	0.17	BRN
Nasmyth Patrick	View near Sevenoaks, Kent	1820	1.03±0.02	82	0.09	NGA
Richard Parkes Bonington	Landscape, Sunset	1826	1.06±0.01	65	0.07	TAS
Joseph Mallord William Turner	Evening: A Windmill at Sunset	1827	1.17± 0.04	92	0.1	TTG
Joseph Mallord William Turner	The Setting Sun over Petworth Park	1827	1.20± 0.03	95	0.11	TTG
Joseph Mallord William Turner	Petworth Park; Sunset ('Glade and Greensward')	1827	1.18±0.01	100	0.1	TTG
Joseph Mallord William Turner	Setting Sun	1827	1.19±0.01	88	0.12	TTG
Joseph Mallord William Turner	Sunset across the Park from the Terrace of Petworth House	1827	1.21±0.04	89	0.12	TTG
Joseph Mallord William Turner	Sunset over the Ridge Seen from the North Pond in Petworth Park	1827	1.01±0.01	100	0.06	TTG
Joseph Mallord William Turner	Evening: A Boat on a River with a Distant Tower	1827	1.15±0.02	100	0.09	TTG
Joseph Mallord William Turner	Sunset: A Boat on a River	1827	1.22±002	87	0.12	TTG
Richard Parkes Bonington	Sunset in the Pays de Caux	1828	1.07±0.03	79	0.07	WLC
Joseph Mallord William Turner	Claudian Harbour Scene	1828	1.17±0.00	95	0.1	TTG
Joseph Mallord William Turner	Cilgerran Castle, Pembrokeshire	1828	1.08±0.01	100	0.08	TTG
Dawe George	Portrait of Fieldmarshal Mikhail Barclay de Tolly	1829	1.30±0.04	87	0.15	HMT
Ferdinand Olivier	Elijah in the Wilderness	1831	1.14±0.00	61	999	NPM
Joseph Mallord William Turner	Fort Vimieux	1831	1.73±0.12	87	0.4	PRV
Joseph Mallord William Turner	Le Havre: Sunset in the Port	1832	1.02±0.01	73	0.27	TTG
Caspar David Friedrich	Swans in the Reeds	1832	1.66±0.06	90	0.31	HMT
Caspar David Friedrich	The Stages of Life	1835	1.11±0.05	85	0.08	MBK
Khrutsky Ivan	Young Woman with Basket	1835	1.16±0.01	90	0.09	HMT
Caspar David Friedrich	The Dreamer (Ruins of the Oybin)	1835	1.70±0.08	90	0.52	HMT
Thomson, Rev. John, of Duddingston	Loch-an-Eilean, Rothiemurchus, Inverness-shire	1835	1.80±0.02	999	0.36	NGA
Hagen, August Mathias	Sea Bay	1835	1.21±0.02	100	0.17	HMT
Joseph Mallord William Turner	Flint Castle	1838	1.11±0.02	90	0.08	PRV
Jean-Baptiste-Camille Corot	Landscape with Lake and Boatman	1839	1.30±0.11	100	0.15	GTT
Joseph Mallord William Turner	Dinant, on the Meuse, from the South	1839	1.03±0.01	999	0.07	TTG
Khrutsky Ivan	View on Yelagin Island in St. Petersburg	1839	1.21±0.05	63	999	HMT
Joseph Mallord William Turner	Mayen in the Eifel	1839	1.09±0.01	999	0.07	TTG
Joseph Mallord William Turner	A View of Metz from the North	c.1839	1.28±0.04	100	0.14	TTG
Christina Robertson	Portrait of Grand Princess Alexandra Nikolayevna	1840	1.11±0.01	999	0.08	HMT
Joseph Mallord William Turner	Distant View of Regensburg from the Dreifaltigkeitsberg	1840	1.06±0.00	86	0.07	TTG
Joseph Mallord William Turner	Sunset on a Lake	1841	1.16±0.01	999	0.09	TTG
Joseph Mallord William Turner	Mont Pilatus: Sunset	1841	1.08±0.01	85	0.07	TTG
Joseph Mallord William Turner	Geneva, the Jura Mountains and Isle Rousseau, Sunset	1841	1.13±0.02	85	0.09	TTG

Table B1. Continued.

Painter's Name	Title of Painting	Year	R/G	SZA	AOD	Gallery*
Joseph Mallord William Turner	Sunset, Lake of Lucerne	1841	1.12±0.01	66	999	TTG
Charles-Gabriel Gleyre	Evening or Lost Illusions	1843	1.16±0.04	83	0.1	KNM
Joseph Mallord William Turner	Yellow Sun over Water	1845	1.21±0.05	90	0.12	TTG
Alexander Ivanov	Via Appia	1845	1.07±0.01	66	999	TRV
Joseph Mallord William Turner	Sunset, over the Water	1845	1.28±0.02	90	0.14	TTG
Eugène Delacroix	Study of Sky Setting Sun	1849	1.19±0.08	88	0.11	LVR
Fitz Hugh Lane	Camden Mountains From the South Entrance to the Harbor	1859	1.14±0.01	87	0.09	FRW
Fitz Hugh Lane	Boston Harbor	1850-52	1.11±0.02	86	0.08	FAB
Gifford Sanford Robinson	Mansfield Mountain	1859	1.10±0.02	82	0.08	MNG
Albert Bierstadt	Coastal View, Newport	1861	1.10±0.00	90	0.08	PRV
Gifford Sanford Robinson	A twilight in the Catskills	1861	1.28±0.01	95	0.14	PRV
Albert Bierstadt	Indian Summer - Hudson River	1861	1.10±0.02	82	0.08	PRV
Gifford Sanford Robinson	A twilight in Adrindacks	1861	1.20±0.01	100	0.11	PRV
Gifford Sanford Robinson	A Lake Twilight	1861	1.04±0.01	90	0.07	PRV
Perov Vasily	The Last Tavern at the City Gates	1868	1.14±0.04	95	0.09	TRV
Eugene Fromentin	Desert Scene	1868	1.32±0.07	999	0.16	HMT
Jean-Leon Gerome	Excursion of the Harem	1869	1.27±0.11	67	999	CHR
Albert Bierstadt	Sunset in Yosemite Valley	1869	1.38±0.07	87	0.17	HGG
Gifford Sanford Robinson	An October Afternoon	1871	1.09±0.01	68	999	FAB
Edgar Degas	Horses in a Meadow	1871	1.05±0.01	999	0.07	NGA
Albert Bierstadt	El Capitan, Yosemite Valley	1875	1.02±0.00	64	999	TLD
Jasper Francis Cropsey	Deer by a Mountain Lake	1875	1.37±0.02	90	0.17	PRV
Jasper Francis Cropsey	Autumn Landscape with Boaters on a Lake	1875	1.13±0.11	82	0.11	NCF
Gifford Sanford Robinson	A Sunset, Bay of New York	1878	1.29±0.08	85	0.14	EVR
Gifford Sanford Robinson	Sunset on the Shore of No Man's Land-Bass Fishing	1878	1.05±0.00	86	0.07	PRV
Gustav Klimt	Fable	1883	1.12±0.02	92	0.09	HCV
Pierre-Auguste Renoir	Seating Girl	1883	1.28±0.06	999	0.15	PRV
William Ascroft	Twilight and Afterglow Effects	1883	2.02±0.05	101.6	0.57	SCN
William Ascroft	Twilight and Afterglow Effects	1884	2.04±0.06	92	0.46	SCN
Breton Jules	The Song of the Lark	1884	1.74±0.05	89	0.35	AIC
William Ascroft	Twilight and Afterglow Effects	1885	1.75±0.05	97	0.36	SCN
Albert Pinkham Ryder	The Temple of the Mind	1885	1.75±0.16	86	0.36	PRV
John Atkinson Grimshaw	An Autumn Idyll	1885	1.28±0.07	90	0.18	RCA
Jasper Francis Cropsey	Evening on the Hudson	1885	1.32±0.08	88	0.2	NCF
William Ascroft	Twilight and Afterglow Effects	1886	1.81±0.03	96	0.37	SCN
Yelland Raymond	Moonrise Over Seacoast at Pacific Grove	1886	1.75±0.04	100	0.33	OKL
Garstin Norman	Haycocks and Sun	1886	1.12±0.02	86	0.13	TTG
Jasper Francis Cropsey	Palisades At Sunset	1887	1.12±0.03	89	0.08	NCF
Jasper Francis Cropsey	View From Artist's Residence, Sunset	1887	1.17±0.03	82	0.1	NCF
Warren W. Sheppard	Moonlight Sail off the Highlands	1888	1.78±0.05	100	0.29	PRV
Millais Sir John Everett	The Moon is Up, and Yet it is not Night	1890	1.24±0.01	999	0.13	NGA
Thomas Hope McLachlan	Evening Quiet	1891	1.30±0.01	999	0.15	TTG
Edgar Degas	Weatfield and Green Hill	1892	1.21±0.01	82	0.12	NSM
Ralph Albert Blakelock	Moonlight	1885-89	1.17±0.03	100	0.09	BKL
Heironymous Bosch	The Path of Life	1500-02	1.13±0.01	81	0.10	LVR
Lambert Sustris	Jupiter and Io	1557-63	1.12±0.01	999	0.09	HMT
Peter Paul Rubens	The Capture of Juliers	1621-25	1.04±0.02	85	0.07	LVR
Gellee, Claude (Le Lorrain)	Embarkation of St Paula Romana at Ostia	1637-39	1.03±0.02	79	0.1	PRD
Jacques Stella	Minerva and the Muses	1640-45	1.11±0.01	999	0.08	LVR
Gellee, Claude (Le Lorrain)	The Disembarkation of Cleopatra at Tarsus	1642-43	1.15±0.02	80	0.27	LVR

Table B1. Continued.

Painter's Name	Title of Painting	Year	R/G	SZA	AOD	Gallery*
Jan Both	Italian Landscape with a Path	1645-50	1.14±0.02	79	0.14	HMT
Aert van der Neer	Landscape with Windmill	1647-49	1.09±0.03	73	0.2	HMT
Sir Joshua Reynolds	Mrs Crewe	1760-61	1.29±0.02	999	0.15	PRV
Sir Joshua Reynolds	Admiral Augustus Keppel	1780	1.34±0.01	999	0.16	TTG
Caspar David Friedrich	View of a Harbour	1815-16	1.86±0.11	90	0.6	SCH
Caspar David Friedrich	Night in a Harbour (Sisters)	1818-20	1.25±0.01	100	0.14	HMT
Caspar David Friedrich	On Board a Sailing Ship	1818-20	1.20±0.02	79	0.17	HMT
Jean-Baptiste-Camille Corot	Poussin's Walk, The Roman Campa	1826-28	1.27±0.02	999	0.14	LVR
Joseph Mallord William Turner	Harbour Scene at Sunrise, possibly Margate	1835-40	1.05±0.02	90	0.07	TTG
Joseph Mallord William Turner	Lausanne: Sunset	1841-42	1.14±0.03	83	0.13	TTG
Jean-Francois Millet	Angelus	1857-59	1.14±0.03	84	0.13	ORS
Francis A Silva	At Sunset	1880-89	1.84±0.41	100	0.38	PRV
Sir Edward Burne-Jones	Chant d'Amour	1868-73	1.21±0.09	999	0.12	MMA
Albert Bierstadt	View of Donner Lake	1871-72	1.07±0.01	76	0.19	FAF
Edgar Degas	Race Horses	1885	1.80±0.02	100	0.36	PHL
Edgar Degas	Horses and Jockeys	1886-90	1.15±0.01	999	0.09	PRV
Albert Pinkham Ryder	Siegfried and the Rhine Maidens	1888-91	1.00±0.02	82	0.09	NGA
Edgar Degas	Field of Flax	1891-92	1.15±0.01	86	0.09	PRV
Caspar David Friedrich	Evening	c. 1824	1.30±0.07	92	0.15	GML MNH
Pieter Brueguel the Elder	Landscape with the fall of Icarus	c.1558	1.04±0.01	89	0.07	RBA
Francesco Vanni	Madonna and Child with St Lucy	c.1600	1.13±0,03	999	0.09	PRV
Johann Konig	Wooded River Landscape with St John the Baptist	c.1610	1.13±0.02	92	0.09	PRV
David Vinckboons	An Officer Preparing His Troops for an Ambush	c.1612	1.26±0.04	82	0.14	PRV
Gellee, Claude (Le Lorrain)	Harbour Scene with Grieving Heliades	c.1640	1.35±0.03	80	0.29	WLR
Caesar van Everdingen	Four Muses and Pegasus on Parnassus	c.1650	1.35±0.02	999	0.16	HTB
Cuyp Aelbert	River-bank with Cows	c.1650	1.07±0.01	63	999	BVB
Jan Both	Italian Landscape with Roman Warriors	c.1650	1.11±0.02	62	999	HMT
Cuyp Aelbert	The Maas at Dordrecht	c.1650	1.05±0.01	60	999	NGA
Caspar David Friedrich	The Grosse Gehege near Dresden	c. 1832	1.07±0.01	90	0.07	GML
Marco Ricci	Landscape with Watering Horses	c.1720	1.00±0.01	80	0.09	GDA
Bellotto Bernardo	View of Pirna from Posta	c.1753	1.29±0.03	71	999	HMT
Wilson Richard	Lake Avernus and the Island of Capri	c.1760	1.16±0.01	90	0.09	TTG
Wilson Richard	River View, on the Arno	c.1760	1.10±0.01	78	0.15	TTG
Thomas Gainsborough	Miss Haverfield	c.1782	1.32±0.11	999	0.16	WLC
Thomas Gainsborough	Boy Driving Cows near a Pool	c.1786	1.14±0.02	76	0.44	TTG
Joseph Mallord William Turner	Windmill on Hill: Valley and Winding River in Middle Distance; Sunset Effect	c.1795	1.08±0.01	84	0.08	TTG
Joseph Mallord William Turner	Sunset over a Calm Sea with a Sailing Vessel, and the Coast of Kent with Reculver Church in the Distance	1796-7	1.32±0.03	88	0.16	TTG
Joseph Mallord William Turner	Snowy Hills beside a Lake: Evening Sky	c.1799-1802	1.06±0.00	90	0.07	TTG
Joseph Mallord William Turner	Study for the Composition of 'Dolbadern Castle'	c.1799-1802	1.08±0.01	100	0.08	TTG
Joseph Mallord William Turner	Barnstaple Bridge at Sunset	c.1813	1.25±0.02	81	0.14	TTG
John Crome	A Windmill near Norwich	c.1816	1.33±0.00	100	0.21	TTG
Caspar David Friedrich	Neubranderburg	c.1817	1.45±0.03	90	0.3	GPL
Caspar David Friedrich	Ships in Greifswald harbour	1818-20	1.74±0.10	100	0.34	GPL
John Crome	Yarmouth Harbour - Evening	c.1817	1.12±0.01	72	0.4	TTG
Joseph Mallord William Turner	Moonlight at Sea (The Needles)	c.1818	1.39±0.02	100	0.23	TTG
Joseph Mallord William Turner	Red Sky and Crescent Moon	c.1818	1.73±0.06	100	0.34	TTG

Table B1. Continued.

Painter's Name	Title of Painting	Year	R/G	SZA	AOD	Gallery*
Caspar David Friedrich	The Sisters on the Balcony	c.1820	1.39±0.12	100	0.18	HMT
Joseph Mallord William Turner	The Bass Rock	c.1824	1.20±0.07	87	0.11	TTG
Joseph Mallord William Turner	Crimson Sunset	c.1825	1.28±0.06	90	0.14	TTG
Joseph Mallord William Turner	Fiery Sunset	c.1825-27	1.23±0.04	100	0.12	TTG
Joseph Mallord William Turner	Sunset over Water	c.1825-27	1.30±0.02	81	0.22	TTG
Joseph Mallord William Turner	Gloucester Cathedral	c.1826	1.15±0.01	100	0.1	TTG
Joseph Mallord William Turner	A Distant View of the Upperton Monument, from the Lake in Petworth Park	c.1827	1.21±0.04	100	0.12	TTG
Joseph Mallord William Turner	Ariccia (?): Sunset	c.1828	1.04±0.01	85	0.06	TTG
Joseph Mallord William Turner	The Lake, Petworth, Sunset	c.1828	1.12±0.02	90	0.13	TTG
Joseph Mallord William Turner	A Ship Aground	c.1828	1.04±0.02	90	0.07	TTG
Joseph Mallord William Turner	The Chain Pier, Brighton	c.1828	1.05±0.01	84	0.07	TTG
Joseph Mallord William Turner	Seacoast with Ruin, probably the Bay of Baiae	c.1828	1.17±0.01	80	0.14	TTG
Joseph Mallord William Turner	Petworth Park: Tillington Church in the Distance	c.1828	1.37±0.03	100	0.17	TTG
Joseph Mallord William Turner	St Michael's Mount from Marazion, Cornwall	c.1828	1.16±0.02	84	0.09	TTG
Joseph Mallord William Turner	Chichester Canal	c.1828	1.14±0.02	90	0.09	TTG
Joseph Mallord William Turner	Classical Harbour Scene	c.1828	1.07±0.00	84	0.08	TTG
Joseph Mallord William Turner	The Lake, Petworth: Sunset, Fighting Bucks	c.1829	1.29±0.04	85	0.15	TTG
Joseph Mallord William Turner	The Lake, Petworth: Sunset, a Stag Drinking	c.1829	1.35±0.02	83	0.2	TTG
Joseph Mallord William Turner	Chichester Canal	c.1829	1.30±0.02	100	0.16	TTG
Joseph Mallord William Turner	Castle Upnor, Kent: Preparatory Study	c.1829-30	1.16±0.01	72	999	TTG
Caspar David Friedrich	The Temple of Juno in Agrigent	c.1830	1.31±0.08	88	0.16	MKK
Joseph Mallord William Turner	Sunset: Study for 'Flint Castle, on the Welsh Coast'	c.1830	1.15±0.01	83	0.14	TTG
Joseph Mallord William Turner	Geneva	c.1830	1.12±0.01	86	0.09	TTG
Joseph Mallord William Turner	Datur Hora Quieti	c.1831-32	1.07±0.01	90	0.08	TTG
Joseph Mallord William Turner	Tornaro (Roger's 'Poems)	c.1832	1.08±0.00	90	0.08	TTG
Joseph Mallord William Turner	A Town on a River at Sunset	c.1833	1.07±0.00	85	0.08	TTG
Joseph Mallord William Turner	Sunset	c. 1833	1.76±0.03	100	0.35	TTG
Kroly Brocky	The Daughters of Istvn Medgyasszay	c.1833	1.12±0.02	999	0.09	PRV
Joseph Mallord William Turner	Sunset over Lake	c.1834	1.23±0.01	100	0.18	TTG
Joseph Mallord William Turner	Sunset	c.1834	1.21±0.02	88	0.17	TTG
Joseph Mallord William Turner	The Arch of Constantine, Rome	c.1835	1.17±0.02	70	999	TTG
Joseph Mallord William Turner	Tivoli: Tobias and the Angel	c.1835	1.11±0.01	83	0.09	TTG
Joseph Mallord William Turner	Sunset: A Fish Market on the Beach	c.1835	1.07±0.01	88	0.08	TTG
Joseph Mallord William Turner	View of Town, with Yellow Sky	c.1839	1.07±0.01	87	0.08	TTG
Joseph Mallord William Turner	Sunset on the Sea	c.1839	1.14±0.01	88	0.09	TTG
Joseph Mallord William Turner	Venice: Sunset	c.1839	1.11±0.00	100	0.09	TTG
Joseph Mallord William Turner	Sunset, with Smoke from a Distant Steamer	c.1840	1.05±0.01	75	0.19	TTG
Joseph Mallord William Turner	Sun Setting over a Lake	c.1840	1.33±0.02	89	0.16	TTG
Joseph Mallord William Turner	Venice: The Campanile of S. Giorgio Maggiore, with S. Maria della Salute on the Right: Sunset	c.1840	1.04±0.01	72	999	TTG
Joseph Mallord William Turner	Sunset over Yellow-Green Waters	c.1840	1.10±0.00	88	0.09	TTG
Joseph Mallord William Turner	S. Maria della Salute and the Dogana: Sunset	c.1840	1.06±0.00	70	999	TTG

Table B1. Continued.

Painter's Name	Title of Painting	Year	R/G	SZA	AOD	Gallery*
Joseph Mallord William Turner	Orange Sunset	c.1840	1.32±0.04	85	0.16	TTG
Joseph Mallord William Turner	The Walhalla, near Regensburg on the Danube	c.1840-42	1.11±0.01	90	0.09	TTG
Albert Bierstadt	Sunset, Deer, and River	c.1868	1.39±0.02	90	0.17	PRV
Edgar Degas	Eugene Manet	c.1874	1.29	89	0.15	PRV
Albert Pinkham Ryder	With Sloping Mast and Dipping Prow	c.1883	1.11±0.02	100	0.08	NAA
Edgar Degas	Landscape on the Orne	c.1884	1.22±0.04	89	0.19	PRV
Elisha Taylor Baker	East river Scene, Brooklyn	c.1886	1.75±0.04	83	999	PRV
Edgar Degas	The Jockey	c.1887	1.32±0.05	90	0.16	PHL
Edgar Degas	Wheatfield and Line of Trees	c.1890-93	1.17±0.04	88	0.1	PRV
Edgar Degas	Landscape: Cows in the Foreground	c.1890-93	1.13±0.01	83	0.09	PRV
Edgar Degas	Landscape by the Sea	c.1895-98	1.12±0.01	999	0.08	PRV
Edgar Degas	The Return of the Herd	c.1896-98	1.18±0.01	72	999	LCS
Sebastien Bourdon	Bacchus and Ceres with Nymphs and Satyrs	1640-60	1.32±0.03	999	0.16	FAB
Alonso Cano	The Dead Christ Supported by an Angel	1646-52	1.19±0.07	90	0.11	PRD
Henry Anderton	Mountain Landscape With dancing Shepherd	1650-60	1.28±0.02	100	0.14	TTG
Francisco Camilo	Adoration of the Magi	1660s	1.16±0.01	100	0.09	BAB
Caesar van Everdingen	Nymphs Offering the Young Bacchus Wine, Fruit and Flowers	1670-78	1.31±0.02	100	0.15	KDE
Luca Carlevaris	The Sea Custom House with San Giorgio Maggiore	1700s	1.12±0.03	97	0.09	PRV
Jan Weenix	Boar Hunt	1703-16	1.18±0.01	999	0.1	ALP
John Crome	Moonrise on the Yare	1811-16	1.40±0.01	100	0.23	TTG
Joseph Mallord William Turner	Study of Sky	1816-18	1.16±0.04	69	999	TTG
Joseph Mallord William Turner	The River; Sunset	1820-30	1.07±0.01	100	0.07	TTG
Joseph Mallord William Turner	Looking out to Sea	1820-30	1.09±0.00	100	0.08	TTG
Joseph Mallord William Turner	Sunlight over Water	1825-30	1.12±0.01	100	0.08	TTG
Joseph Mallord William Turner	The Scarlet Sunset	1830-40	2.40±0.17	87	999	TTG
Alexander Ivanov	The Appearance of Christ to the People	1837-57	0.90±0.03	100	0.03	TRV
Ziem, Felix Francois Georges Philibert	Harbour at Constantinople	1880s	1.28±0.01	87	0.14	HMT
Arkhip Kuinji	Sunset	1885-90	1.84±0.06	999	0.31	RSS
Edgar Degas	Horses and Jockeys	1886-90	1.35±0.02	80	0.17	PRV
Arkhip Kuinji	Sunset	1890-95	2.26±0.03	88	999	RSS
Warren Sheppard	Sunset Sail	1890s	1.21±0.03	100	0.13	SPF
William Hogarth	Conversation Piece (Portrait of Sir Andrew Fountaine with Other Men and Women)	c. 1730-35	1.20±0.05	999	0.12	PHL
Smith George of Chichester	Classical Landscape	c.1760-70	1.06±0.09	86	0.07	NGA
Wilson Richard	Landscape with Bathers, Cattle and Ruin	c.1770-75	1.07±0.02	88	0.07	TTG
Joseph Mallord William Turner	Sunset	c.1820-30	1.09±0.01	100	0.08	TTG
Joseph Mallord William Turner	Running Wave in a Cross-Tide: Evening	c.1820-30	1.27±0.04	100	0.14	TTG
Joseph Mallord William Turner	The Distant Tower: Evening	c.1820-30	1.09±0.02	85	0.08	TTG
Joseph Mallord William Turner	Twilight over the Waters	c.1820-30	1.09±0.01	100	0.08	TTG
Joseph Mallord William Turner	A Ruin: Sunset	c.1820-30	1.21±0.03	100	0.13	TTG
Joseph Mallord William Turner	Sunset	c.1820-30	1.11±0.02	100	0.09	TTG
Joseph Mallord William Turner	River: Sunset	c.1820-30	1.08±0.01	70	999	TTG
Joseph Mallord William Turner	The Line of Cliffs	c.1820-30	1.17±0.01	84	0.1	TTG
Joseph Mallord William Turner	River with Trees: Sunset	c.1820-30	1.10±0.00	100	0.09	TTG
Joseph Mallord William Turner	River Scene: Sunset	c.1820-30	1.34±0.15	100	0.16	TTG
Joseph Mallord William Turner	Studies of Skies	c.1820-30	1.14±0.01	100	0.1	TTG
Joseph Mallord William Turner	Evening	c.1820-30	1.12±0.02	73	999	TTG

Table B1. Continued.

Painter's Name	Title of Painting	Year	R/G	SZA	AOD	Gallery*
Joseph Mallord William Turner	The Castle by the Sea	c.1820-30	1.09±0.00	100	0.09	TTG
Joseph Mallord William Turner	Sunset	c.1820-30	1.11±0.01	100	0.09	TTG
Joseph Mallord William Turner	Study for 'The Golden Bough'	c.1820-30	1.12±0.02	79	0.13	TTG
Joseph Mallord William Turner	Sunset over the Sea	c.1820-30	1.10±0.00	86	0.08	TTG
Joseph Mallord William Turner	Rochester Castle and Bridge	c.1820-30	1.11±0.00	90	0.09	TTG
Joseph Mallord William Turner	Sunset	c.1820-30	1.11±0.01	100	0.09	TTG
Joseph Mallord William Turner	The Yellow Sky	c.1820-30	1.10±0.01	100	0.09	TTG
Joseph Mallord William Turner	A Pink Sky above a Grey Sea	c.1822	1.22±0.07	100	0.13	TTG
Caspar David Friedrich	Moonrise by the Sea	c.1822	1.32±0.02	100	0.16	NGB
Joseph Mallord William Turner	A Stormy Sunset	c.1822	1.13±0.01	100	0.09	TTG
Joseph Mallord William Turner	Fiery Sunset	c.1825-27	1.30±0.03	100	0.15	TTG
Joseph Mallord William Turner	Sunset over Water	c.1825-27	1.06±0.00	82	0.08	TTG
Joseph Mallord William Turner	Sunset over a City	c.1826-36	1.19±0.01	100	0.12	TTG
Joseph Mallord William Turner	Regulus	c.1827-37	1.01±0.01	86	0.06	TTG
Caspar David Friedrich	Sunset (Brothers)	c.1830-35	1.66±0.05	86	0.37	HMT
Caspar David Friedrich	Mountainous River Landscape (Night Version)	c.1830-35	1.78±0.04	100	0.35	SMK
Sir Augustus Wall Callcott	Dutch Landscape with Cattle	c.1830-40	1.05±0.00	63	999	TTG
Joseph Mallord William Turner	Sunset. (?Sunrise)	c.1835-40	1.33±0.05	100	0.21	TTG
Joseph Mallord William Turner	A Lurid Sunset	c.1840-45	1.31±0.07	100	0.15	TTG
Joseph Mallord William Turner	Sunset Seen from a Beach with Breakwater	c.1840-45	1.32±0.03	100	0.16	TTG
Joseph Mallord William Turner	The Rigi	c.1841	1.12±0.02	100	0.09	TTG
Joseph Mallord William Turner	Sunset From the Top of the Rigi	c.1844	1.04±0.02	999	0.07	TTG
Ralph Albert Blakelock	Landscape with Trees	c.1880-90	1.49±0.11	100	0.27	MAR
Ralph Albert Blakelock	Edge of the Forest	c.1880-90	1.36±0.09	100	0.22	BKL
Ralph Albert Blakelock	Afternoon Light	c.1880-90	1.32±0.06	90	0.21	MAR
Gustav Klimt	Sappho	1888-90	1.65±0.05	100	0.25	HCV
Joseph Mallord William Turner	Sea Monsters and Vessels at Sunset	c.1845	1.39±0.03	100	0.18	TTG
Joseph Mallord William Turner	Yellow and Blue Sunset over Water	c.1845	1.07±0.00	81	0.1	TTG
Joseph Mallord William Turner	Sunset at Ambleteuse	c.1845	1.24±0.03	100	0.13	TTG
Joseph Mallord William Turner	Sunset	c.1845	1.21±0.02	100	0.13	TTG
Joseph Mallord William Turner	Yellow Sunset	c.1845	1.32±0.07	85	0.16	TTG
Joseph Mallord William Turner	The Red Rigi: Sample Study	c.1841-42	1.12±0.02	69	999	TTG
Albert Bierstadt	South and North Moat Mountains	c.1862	0.99±0.01	60	999	PRV
Albert Bierstadt	White Horse and Sunset	c.1863	1.22±0.03	100	0.13	BBH
Albert Bierstadt	Evening on the Prarie	c.1870	1.07±0.01	91	0.08	TBM
Albert Bierstadt	Sacramento River Valey	c.1872	1.06±0.01	88	0.08	TBM

Table B2. Galleries abbreviations:

AIC: The Art Institute of Chicago, USA	MMA: The Metropolitan Museum of Art, New York City, USA
ALP: Alte Pinakothek, Munich, Germany	MNG: Manoogian Collection
AMA: Allen Memorial Art Museum, Oberlin, Ohio, USA	NAA: National Museum of American Art, USA
BAB: Museo de Bellas Artes, Bilbao, Spain	NCF: Newington Cropsey Foundation Gallery of Art
BBH:Buffulo Bill Historical Center, USA	NGA: National Gallery of Art, Washington, USA
BKL: Brooklyn Museum, NY, USA	NGB: Nationalgalerie, Berlin, Germany
BRN: British National Museum, London	NGL: The National Gallery, London, UK
BVB: Museum Boijmans Van Beuningen, Rotterdam, The Netherlands	NGO: The National Gallery, Oslo, Norway
CHR: Chrysler Collection, Norfolk, Virginia, USA	NPM: Neue Pinakothek, Munich, Germany
CHW: Castle Howard, Yorkshire, UK	NSM: Norton Simon Foundation, Pasadena
CTI: Courtauld Institute Galleries, London, UK	OKL: The Oakland Museum of California, USA
EVR: Everson Museum of Art, USA	ORF: Oskar Reinhart Foundation, Winterthur
FAB: Museum of Fine Arts, Boston, USA	ORS: Musee d'Orsay, Paris, France
FAB: Museum of Fine Arts, Budapest, Hungary	PHL: Philadelphia Museum of Art, USA
FAF: Fine Arts Museums of San Francisco, California, USA	PLP: Palazzo Pitti, Galleria Palatina, Florence, Italy
FGA: Fogg Art Museum, Harvard University, Cambridge, Massachusetts	PRD: Museo del Prado, Madrid, Spain
FLK: Museum Folkwang, Essen, Germany	PRV: Private collection
FRW: Farnsworth Art Museum, Rockland, ME.	RBA: Musee Royal des Beaux Arts, Antwerp, Belgium
GDA: Gallerie dell'Accademia, Venice, Italy	RBA: Musees Royaux des Beaux-Arts, Brussels, Belgium
GML: Gemaldegalerie Neue Meister, Staatliche Kunstsammlungen, Dresden	RCA:Russell-Cotes Art Gallery and Museum, Bournemouth, England
GPL: Griefswald, Pommersches Landmuseum, Germany	RCL:Royal Collection, London, UK
GTT: The J. Paul Getty Museum, Malibu, CA, USA	RPC: Musee Rupert de Chievres, Poitiers
HAU: Herzog Anton Ulrich-Museum, Brunswick	RSS: The Russian Museum, St-Petersburg, Russia
HCV: Historical Museum of the City of Vienna, Vienna, Austria	SCH: Schloss Scharlattenburg, Stiftung Preussische Berlin, Germany
HGG: Haggin Museum, USA	SCN: Sciencemuseum, London, UK
HMA: Hiroshima Museum of Art, Japan	SFS: Museum Schloss Fasanerie, Eichenzell
HMT: The Hermitage Museum, St. Petersburg, Russia	SMK: Staatliche Museen Kassel
HTB: Huis ten Bosch, The Hague	SPF: Susan Powell Fine Art, NY, USA
KDE: Kunstmuseum Dusseldorf im Ehrenhof, Dusseldorf, Germany	STL: Staatliche Museen, Berlin, Germany
KNH: Kunsthalle, Hamburg, Germany	TAS: Thomas Agnew & Sons Ltd., UK
KNH: Kunsthistorisches Museum, Vienna, Austria	TBM: Thyssen-Bornemisza Museum, Spain
KNM: Kunstmuseum, Winterthur	TLD: Toledo Museum of Art, USA
LCS: Leicestershire Museum and Art Gallery	TRV: The Tretyakov Gallery, Moscow, Russia
LVR : Musee du Louvre, Paris, France	TTG: The TTG
MAR: Memorial Art Gallery of the University of Rochester, USA	WLC: Wallace Collection, London, UK
MBK: Museum der Bildenden Kunste, Leipzig, Germany	WLR: Wallraf-Richartz Museum, Cologne, Germany
MKK: Museum fur Kunst und Kulturgeschichte, Dortmund	

Acknowledgements. This work has been partially supported by EU GOCE-CT-2004-003893 and while one of us was a post doc scholar from IKY at the National Technical University of Athens. The authors are indebted to B. Mayer, H. Graf, D. Stevenson and two anonymous reviewers for their valuable comments and suggestions.

Edited by: F. J. Dentener

References

Anderson, G., Clough, S., Kneizys, F., Chetwynd, J., and Shettle, E.: AFGL Atmospheric Constituent Profiles (0–120 km), Air Force Geophysics Laboratory, AFGL-TR-86-0110, Environmental Research Paper No. 954, 1986.

Bockemuhl, M., "Turner", Taschen, 2000.

Clausen, H. B. and Hammer, C. U.: The Laki and Tambora eruptions as revealed in Greenland ice cores from 11 locations, An-

nals of Glaciology 10, 16–22, 1988.
Deirmendijian, D.: On Volcanic and Other Particulate Turbidity Anomalies, Advan. Geophys., 16, 267–296, 1973.
Hammer, C. U., Clausen, H. B., and Dansgaard, W.: Greenland ice sheet evidence of post-glacial volcanism and its climatic impact, Nature, 288, 230–235, 1980.
Humphreys, W. J.: Physics of the air, New York and London: McGraw-Hill, 1940.
Jameson, D. and Hurvich, L. M.: Some quantitative aspects of an opponent-colors theory I, Chromatic responses and spectral saturation, J. Opt. Soc. Am., 45, 546–552, 1955.
Kylling, A., Bais, A. F., Blumthaler, M., Schreder, J., Zerefos, C. S., and Kosmidis E.: Effect of aerosols on solar UV irradiances during the Photochemical Activity and Solar Ultraviolet Radiation campaign, J. Geophys. Res., 103(20), 26 051–26 060, 1998.
Lamb, H. H.: Volcanic dust in the atmosphere, with a chronology and assessment of its meteorological significance, Philos. Trans. R. Soc. London, Ser. A, 266, 425–533, 1970.
Lamb, H. H.: Supplementary volcanic dust veil assessments, Climate Monitor, 6, 57–67, 1977
Lamb, H. H.: Uptake of the chronology of assessments of the volcanic dust veil index, Climate Monitor, 12, 79–90, 1983.
Mayer, B. and Kylling, A.: Technical note: The LibRadtran software package for radiative transfer calculations: Description and examples of use, Atmos. Chem. Phys., 5, 1855–1877, 2005
Mayer, B. and Emde, C.: Comment on "Glory phenomenon informs of presence and phase state of liquid water in cold clouds" by Nevzorov, A. N., Atmos. Res., 84, 410–419, 2007
Newhall, C. G. and Self, S.: The volcanic explosivity index (VEI): an estimate of explosive magnitude for historical volcanism, J. Geophys. Res., 87, 1231–1238, 1982.
Nicolet, M.: On the molecular scattering in the terrestrial atmosphere: An empirical formula for its calculation in the homosphere, Planet. Space Sci., 32, 1467–1468, 1984.
Robertson, A., Overpeck, J, Rind, D., Mosley-Thompson, E., Zielinski, G., Lean, J., Koch, D., Penner, J., Tegen I., and Healy, R.: Hypothesized climate forcing time series for the last 500 years, J. Geophys. Res., 106(D14), 14 783–14 803, 2001.
Robock, A. and Free M. P.: The volcanic record in ice cores for the past 2000 years, in Climatic Variations and Forcing Mechanisms for the Past 2000 Years, edited by: Jones, P. D. and Bradley, R. S., Springer-Verlag, New York, 533–546, 1996.
Robock, A. and Free, M. P.: Ice cores as an index of global volcanism from 1850 to the present, J. Geophys. Res., 100, 11 549–11 567, 1995.
Robock, A.: A latitudinally dependent volcanic dust veil index, and its effect on climate simulations, J. Volcanol. Geotherm. Res., 11, 67–80, 1981.
Robock, A.: Volcanic eruptions and climate, Rev. Geophys., 38, 191–219, 2000.
Sandick, R. A.: In het rijk van Vulcaan. De uitbarsting van Krakatau en hare gevolgen, Zutphen, W.J. Thieme & Cie, 1890.
Sapper, K.: Beitrage zur Geographie der tatigen Vulkane, Z. Vulk, Berlin 3, 65–197, 1917.
Sato, M., Hansen, J. E., McCormick, M. P., and Pollack, J. B.: Stratospheric aerosol optical depths 1850–1990, J. Geophys. Res., 98, 22 987–22 994, 1993.
Schefrin, B. E. and Werner, J. S.: Loci of spectral unique hues throughout the life span, J. Opt. Soc. Am. A, 7, 305–311, 1990.
Shaw, N.: Manual of meteorology, vol. II: Comperative meteorology, Cambridge University Press, 1936.
Shevell, S. (Ed.): The science of color, 2nd edition, Optical Society of America, Elsevier, 2003.
Stamnes, K., Tsay, S.-C., Wiscombe, W., and Jayaweera, K.: Numerically stable algorithm for discrete-ordinate-method radiative transfer in multiple scattering and emitting layered media, Appl. Optics, 27, 2502–2509, 1988.
Stothers, R. B.: Major optical depth perturbations to the stratosphere from volcanic eruptions: Pyrheliometric period 1881–1960, J. Geophys. Res., 101, 3901–3920, 1996.
Stothers, R. B.: Mystery cloud of AD 536. Nature 307, 344–345, 1984a.
Stothers, R. B.: The great Tambora eruption in 1815 and its aftermath, Science, 224, 1191–1198, 1984b.
Symons, G. J. (Ed.): The eruption of Krakatoa and subsequent phenomena, 494pp. London, Trubner and Co., 1888.
Wyszecki, G. and Stiles, W. S.: Color Science – Concepts and Methods, Quantitative Data and Formulae, 2nd edn. New York: John Wiley and Sons, 1982.
Zielinski, G. A.: Use of paleo-records in determining variability within the volcanism-climate system, Quat. Sci. Rev., 19, 417–438, 2000.
Zielinski, G. A.: Stratospheric loading and optical depth estimates of explosive volcanism over the last 2100 years derived from the GISP2 Greenland ice core, J. Geophys. Res., 100, 20 937–20 955, 1995.